STTC analysis of spontaneous calcium imaging recordings

Vassilis Kehayas, Anna Palagina, Orestis Mousouros, Ioannis Smyrnakis, Stelios M. Smirnakis, Maria Papadopouli

2019-09-19

Technical Report

Introduction

Based on anatomical measurements, it is expected that most neighbouring pyramidal neurons in the cortex are not connected, and those that are will be weakly connected (Braitenberg and Schüz 1998). Indeed, most connections between neurons in L2/3 are weak (Song et al. 2005; Perin, Berger, and Markram 2011; Cossell et al. 2015). However, there are infrequent strong connections that link neurons with similar response properties (Ko et al. 2011; Cossell et al. 2015).

Spike correlations reflect that underlying structural connectivity distribution by exhibiting very small average magnitudes, even for neurons with similar receptive fields (Ecker et al. 2010), which arise due to the combined effect of the restricted extend of common inputs and the action of inhibitory neurons (Ecker et al. 2010; Renart et al. 2010).

It is still an open question whether a description based on correlations observed in spontaneous cortical networks can help to characterize their inherent structure. We expect, though, that some structure is imprinted into the network either through common wiring rules (Yoshimura, Dantzker, and Callaway 2005; Zador 2019) or through the combined effect of natural input statistics and contextual, or "internal state", information (Ringach 2009), that will manifest at the level of spontaneous neuronal correlations. A way to examine the extent to which this is true is to examine the network's topology under multiple scales of correlation and compare it to that of otherwise equivalent reference networks that either lack any structure or display regular topology (Watts and Strogatz 1998). So far studies of network topology have been limited to small-scale *in vitro* studies, that may have missed network structure that manifests itself when looking at larger topological scales.

The range and distribution of inter-neuronal spike correlations has been a matter of controversy, in part due to the influence of the firing rate on the chosen correlation measure (Cohen and Kohn 2011). For this reason, the correlation measure has to be chosen carefully to take into consideration of the underlying characteristics of spike trains. For relatively long time-series, Spike Time Tiling Coefficient (STTC) is superior to commonly used measures, including Pearson, as it accounts for relative

time shifts, local fluctuations of neural activity or noise, and the presence of periods without firing events (Cutts and Eglen 2014).

We chose to calculate STTC based on Δt values within $[0, 600]$ ms as the structure of the network is shaped by the relatioships between excitatory and inhibitory activity that show co-activation patterns within latency ranges in the ± 600 ms interval, (Palagina, Meyer, and Smirnakis 2019) as well as based on GCaMP6 kinetics.(Chen et al. 2013)

Estimation of STTC

To quantify the degree of correlation between firing events of two neurons A and B we used a modified version of the spike time tiling coefficient (STTC) (Cutts and Eglen 2014) which was originally defined as:

$$STTC_{A,B} = \frac{1}{2}\left(\frac{P_A - T_B}{1 - P_A T_B} + \frac{P_B - T_A}{1 - P_B T_A}\right) (¿ eq : sttcCutts)$$

where T_A the proportion of the recording duration within an interval Δt around each firing event of neuron A, P_A the proportion of firing events of neuron A found within an interval Δt around each firing event of neuron B, and likewise for T_B and P_B. This correlation index is robust against varying firing rates and has only one free parameter, the time window Δt.

To incorporate the temporal order of the firing events of two neurons A and B, we developed the directional STTC:

¿

where $T_{A^{+¿}¿}$ is the fraction of the total recording duration within a time window Δt after each spike of A $T_{B^{-¿}¿}$ is the fraction of the total recording duration within a time window Δt before each spike of B, $P_A^{B^{-¿}¿}$ is the proportion of firing events of A within a time window Δt before each firing of B, and $P_B^{A^{+¿}¿}$ is the proportion of firing events of B within a time window Δt after each firing event of A.

The directional STTC retains the desirable properties of the original STTC, while providing information on the temporal direction of correlation between two neurons. We will use the term “STTC” to exclusively refer to the directional STTC from here on. We chose to evaluate the STTC between neurons in our datasets with three different values for Δt based on physiological considerations: $\{0, 0.3, 0.6\}$ secs. As data from different mice were acquired with different sampling rates, we chose the integer number of frames for each mouse that came closest to the three different parameter values. In all cases but one, the real Δt value was equal to the target duration with a single significant digit precision. In the remaining case, one animal

had its real frame duration closer to 0.5 than 0.6 with single significant digit precision.

To evaluate the extend to which the observed STTC values could arise by sequences with the same number of firing events without any temporal structure, we circularly shifted the firing events of each neuron A by a uniformly sampled integer number of imaging frames within the interval $[1, n_{frames}]$ 500 hundred times independently, where n_{frames} the total number of imaging frames. From these 500 iterations we obtained a null distribution of STTC values for each pair of neurons.

The Z-score of each edge between neurons A and B is defined as

$$Z_{A,B} = \frac{STTC^{obs}_{A,B} - \overline{STTC^{null}_{A,B}}}{\sigma^{null}_{A,B}} \quad (¿\, eq: zScore)$$

The Z-score quantifies the distance of the observed STTC value, $STTC^{obs}_{A,B}$, from the mean of the null STTC distribution, $\overline{STTC^{null}_{A,B}}$ which should be close to 0, in units of standard deviations of the null STTC distribution, $\sigma^{null}_{A,B}$.

To evaluate the overall trend of the percentage of edges above different Z-score thresholds and with different Δt values we fitted the model described in Equation (4):

$$\begin{aligned}
o_i &\sim Binomial(n_i, p_i) \\
logit(p_i) &\; ¿\, \alpha + a_{FOV_i} + \beta_1 \Delta t_i + \beta_2 Threshold_i + \beta_3 (\Delta t_i \cdot Threshold_i) \\
\alpha &\sim Normal(3, 1) \\
a_{FOV} &\sim Normal(0, \sigma_{FOV}) \\
\sigma_{FOV} &\sim StudentT(3, 0, 3) \\
\beta_1 &\sim StudentT(3, 0.1, 3) \\
\beta_2 &\sim StudentT(3, -0.1, 3) \\
\beta_3 &\sim StudentT(3, 0, 3)
\end{aligned} \qquad (¿\, eq: pcEdgeBinomialModel)$$

Graph theoretical analysis

Each FOV's network was represented as a graph $G(N, E)$, where N the set of the graph's nodes and E the set of the graph's edges, with a square adjacency matrix A whose each element $\alpha_{i,j}$ was a boolean value, with 1 if neurons i, j were connected and 0 otherwise. We assigned $\alpha_{i,j}$ values based on whether the observed STTC value exceeded each Z-threshold. This matrix was symmetrical when graphs were considered as undirectional, with $\alpha_{i,j}$ filled with 1 if either $E_{i \to j}$ or $E_{j \to i}$ existed, i.e. had an STTC value greater than the Z-threshold. For directional graphs, $\alpha_{i,j}$ were filled with 1 if, and only if, $E_{i \to j}$ existed.

The undirected degree of node i was defined as

$$k_i = \sum_{j \in N} \alpha_{ij} (¿ eq : undirectedDegree)$$

and the directed in- and out-degree as:

$$k_i^{OUT} = \sum_{j \in N} \alpha_{i \to j} (¿ eq : outDegree)$$

$$k_i^{¿} = \sum_{j \in N} \alpha_{j \to i} (¿ eq : inDegree)$$

The undirected shortest path length between nodes i and j was defined as:

$$l_{ij} = \sum_{\alpha_{ij} \in g_{ij}} \alpha_{ij} (¿ eq : undirectedPathLength)$$

where g_{ij} is the shortest path between i and j. The shortest path lengths of disconnected pairs were set to ∞ and were excluded from calculations of summary statistics on the shortest path lengths among nodes of the same graph.

The undirected clustering coefficient of node i is defined as

$$C_i = \frac{\sum_{(j,h) \in N, j \neq i, h \neq (i,j)} \alpha_{ij} \alpha_{ih} \alpha_{jh}}{k_i (k_i - 1)} (¿ eq : ccUndirected)$$

and the directed clustering coefficient of node i is defined as

$$C_i = \frac{1}{2} \frac{\sum_{(j,h) \in N, j \neq i, h \neq (i,j)} (¿ \alpha_{ij} + \alpha_{ji})(\alpha_{ih} + \alpha_{hi})(\alpha_{jh} + \alpha_{hj})}{(k_i^{out} + k_i^{¿})(k_i^{out} + k_i^{¿} - 1) - 2 \sum_{j \in N} \alpha_{ij} \alpha_{ji}} (¿ eq : ccFagiolo) ¿$$

For all graph theory analysis, only connected components with ¿ 2 nodes were considered.

A graph follows *a small-world topology*, if it has a large clustering coefficient that is close to that of an equivalent lattice network but a small average shortest path as should an equivalent random network (Watts and Strogatz 1998). In order to evaluate the extend to which the network of each FOV follows the small-world topology, we calculated three small-world indices that can be found in the literature:

$$\sigma = \frac{\frac{C}{C_r}}{\frac{L}{L_r}} (¿ eq : swiHumphries)$$

where C the clustering coefficient of the observed data, C_r the clustering coefficient of the shuffled graphs, L the average shortest path of the observed data, and L_r the average shortest path of the shuffled graphs (Humphries and Gurney 2008),

$$\omega = \frac{L_r}{L} - \frac{C}{C_l} (¿ eq : swiTelesford)$$

where C_l is the clustering coefficient of an equivalent lattice graph (Telesford et al. 2011), and

$$v = \frac{L - L_l}{L_r - L_l} \times \frac{C - C_r}{C_l - C_r} (¿ eq : swiNeal)$$

(Neal 2017).

Shuffled graphs were produced based on the Erdös-Rényi topology using the same number of nodes and edges as each of the connected components of the observed graphs, $¿ N \vee ¿$ and $¿ E \vee ¿$, while the IDs of each of an edge's pair of nodes where uniformly assigned with self-connections disallowed, 100 times independently. Lattice graphs were generated according to the ring lattice topology, in which each node was connected with an equal number of neighbours, by progressively filling the k-diagonals and corners of an empty graph's adjacency matrix, until the total number of edges matched or exceeded that of the observed graph. A pruning step followed to reduce the number of edges to that in the observed graph, by uniformly selecting a number of edges to extinguish equal to the excess of the intermediate adjacency matrix's number of edges compared to the observed. Only for connected components for which $¿ E \vee \geq \vee N \vee ¿$ held was the ring lattice construction attempted.

Basic description of the data

Number of mice, FOVs, OGB/GCaMP, average/range frame duration, average/range recording duration Measurements: average/range firing rate, average/range number of neurons per FOV In OGB mice there were average/range number of interneurons

Performance Analysis

The following paragraphs present each main finding with plots that support it.

1. Statistically significant STTC values and edges.

Based on the STTC measure of correlation, we identified inter-neuronal connections at different magnitudes of correlation. To examine whether the observed STTC values can be explained by random correlations between neurons that fire the same number of events as those observed, we circularly shifted the event trains of one each pair's neurons by a uniformly random number of imaging frames. The resulting null distributions had a mean STTC of ≈ 0 and spread very little compared to the observed distributions (Figure 1). The observed distribution had most of its density occupy positive STTC values, up to about 0.3.

The observed distribution had most of its density occupy positive STTC values, up to about 0.25. In the example animal that is shown in Figure 1 the median was ≈ 0.034 and 4% of values were >0.1.

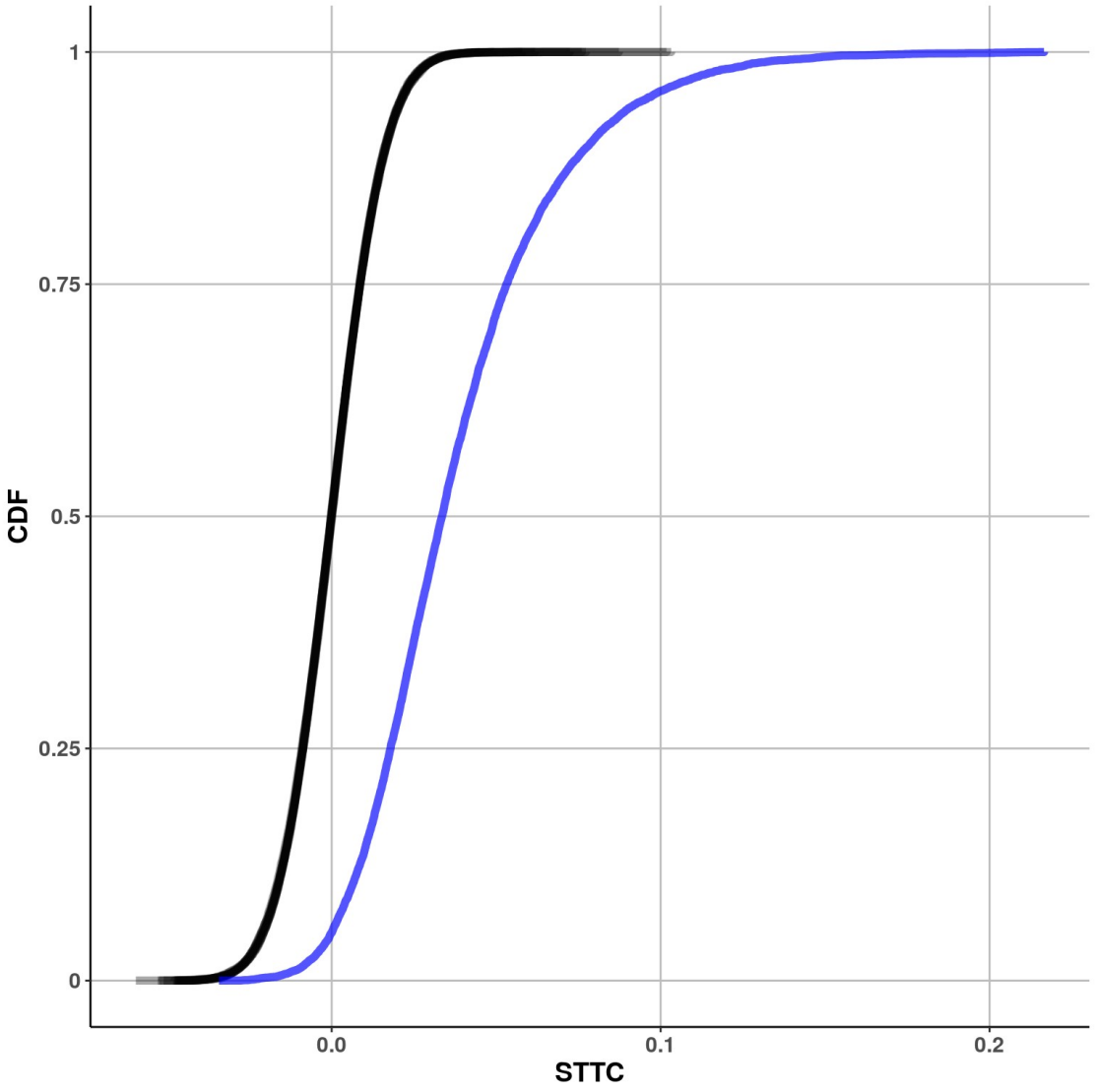

Figure 1: ***Observed versus circularly-shifted STTC distributions for an example animal****: The blue line corresponds to the STTC distribution obtained from the observed data and the black lines to the STTC distribution from 10 randomly-sampled distributions out of the 500 total distributions obtained by circularly-shifting the observed event trains. The STTC was calculated with the same* $\Delta t \approx 0.3$ *for both distributions.*

2. The extend to which the observed STTC differs from the null distribution depends on the size of the temporal integration window.

In order to translate each edge's STTC values to a range that signifies deviation from the null distribution as defined above, we calculated the Z-score of the observed

STTC values with respect to the null's mean and standard deviation. The relationship between STTC and its Z-score was linear for all Δt tested (Figure 2). As the parameter Δt increases, the slope of the correlation decreases, since the differences between the observed and the null STTC values are less pronounced for higher Δt. In addition, the variance of the STTC Z-score is increased as the STTC is increased, leading to heteroscedasticity, which is more pronounced for higher values of Δt. These findings indicate that inter-neuronal correlations can be better estimated using shorter windows of temporal integration.

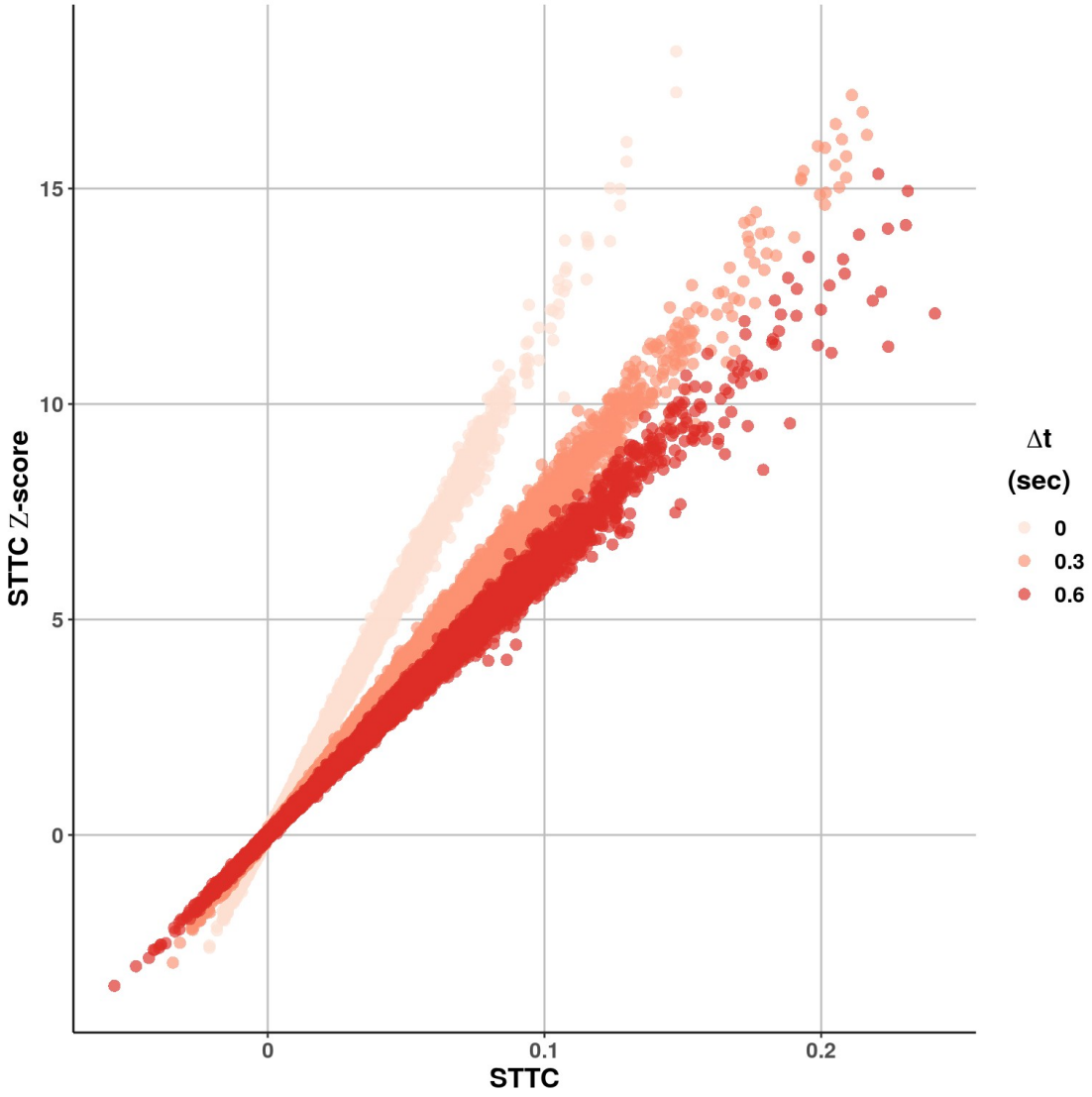

Figure 2: ***STTC versus its*** Z***-score by*** Δt ***for an example mouse****.*

3. Robust identification of edges for sufficient recording durations.

We examined the robustness of the STTC estimation in time by artificially considering increasingly larger recording durations of the whole recording duration we had available. In Figure 3 we see that the observed STTC for increasingly larger

recording durations appears relatively stable across recording durations for each FOV (Figure 3). We also found that more than 75% of edges were between the same nodes when comparing consecutively increasing sizes of windows larger than 9 minutes for most fields of view (FOVs) across all Z-thresholds, a result that did not appreciably differ when using $\Delta t \approx 0$ or ≈ 0.3 seconds (Figure 4). The fact that both the STTC values and the identities of the nodes between which edges are formed remain stable as we consider increasingly larger recording durations provides evidence that the majority of edges we report are reliably detected.

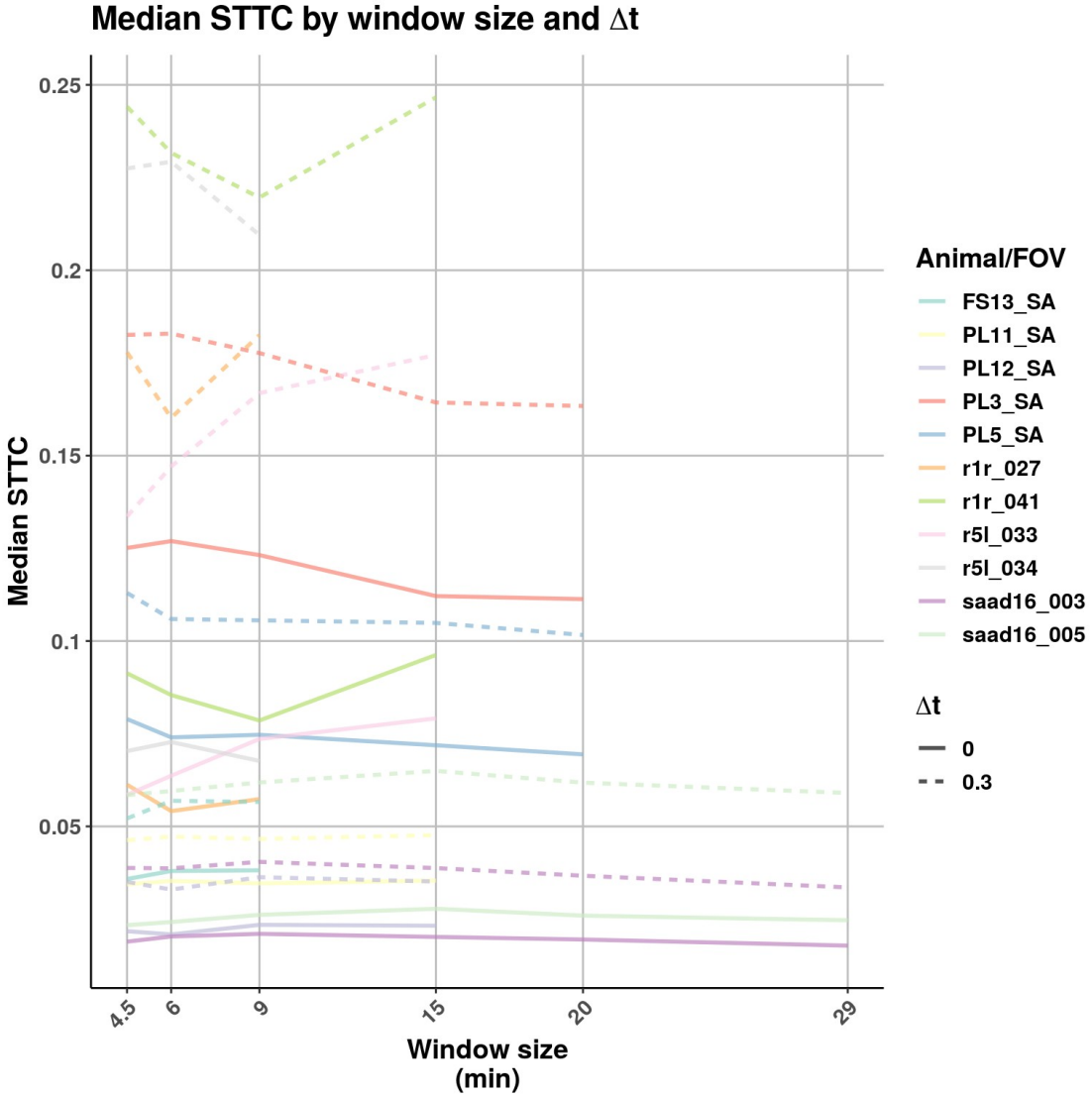

Figure 3: ***Median STTC by window size and*** *Δt: Window sizes were selected to maximize the number of times each animal is included.*

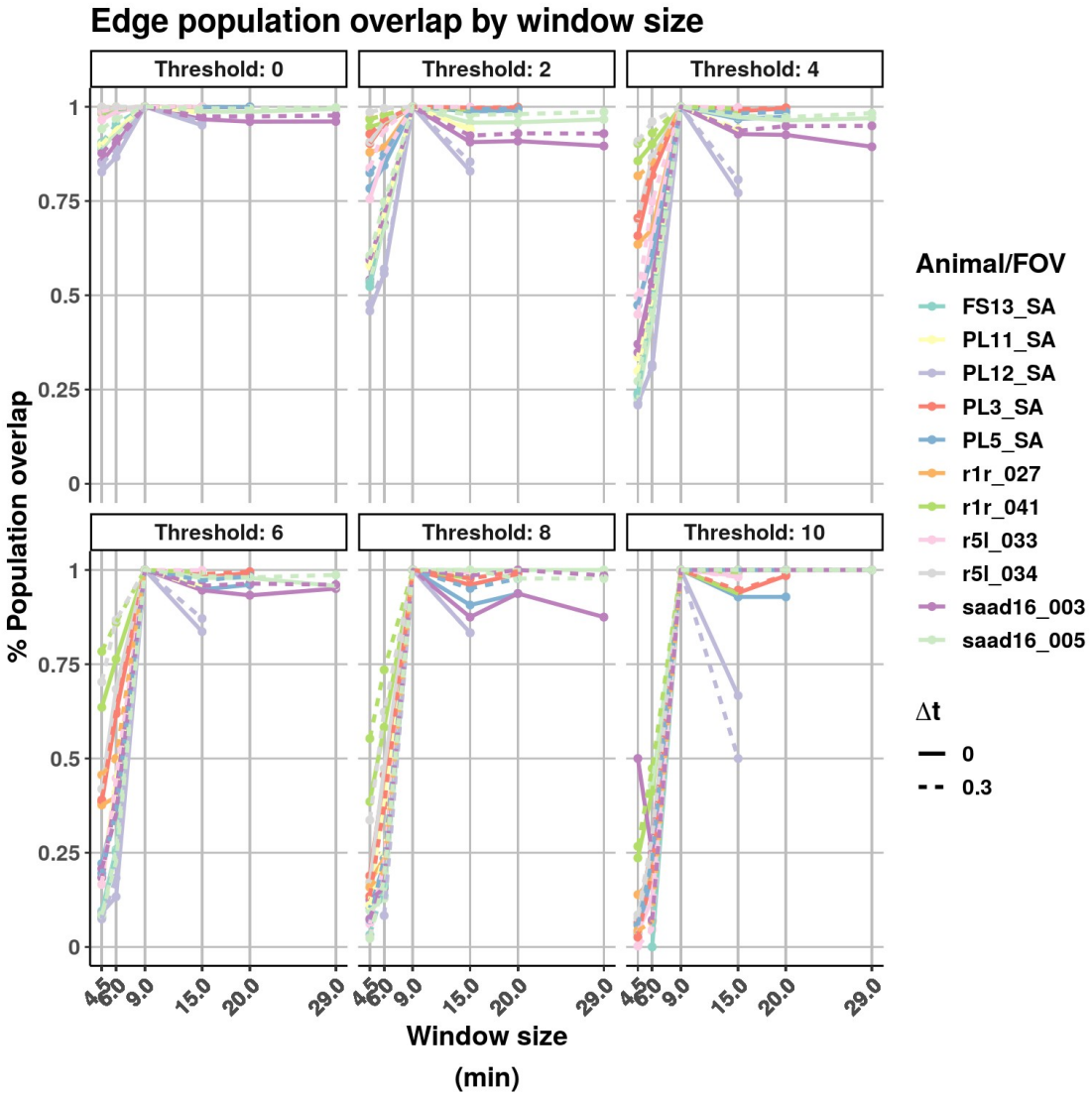

Figure 4: ***Percent of edges above threshold by window size and*** *Δt: Window sizes were selected to maximize the number of times each animal is included.*

Parameters

4. The network manifests structure beyond what is expected by its number of events within the recording period irrespective of how high we set the correlation threshold for the existence of an edge.

As an estimate of network stability, we calculated the percent of edges that have an STTC value above increasing values of the STTC's Z-score. We expected this percentage to be larger than that calculated based on the null distribution and to drop smoothly as we increased the Z-threshold. The percent of edges above threshold as the threshold increases does not change appreciably for different values of Δt assuming a linear model, although there is a higher percentage of edges

for thresholds $\gtrapprox 4$ for $\Delta t \approx 0.3$ compared to both $\Delta t = 0$ and $\Delta t \approx 0.6$ sec (0.055 ± 0.014, $mean \pm 95\% CI$ for $\Delta t \approx 0.3$ *vs* $\Delta t \approx 0.6$, Figure 5). The average inflection point of percentage of edges drop is at Z-threshold of ≈ 4.8 and is found to be larger than that calculated based on the null distribution for all thresholds (Figure 6). From this evidence, we can conclude that more edges, compared to what is expected by an equal number of events randomly shifted in time, can be found for any correlation level up to which we choose to restrict the network. This indicates that the majority of edges assigned based on firing event correlation are integral parts of the network structure whose existence cannot be explained by a distribution of the same number of events in time that does not respect the existing correlations, and that this is the case irrespective of the correlation threshold we choose. The fact that a higher percentage of edges persists for a temporal integration window of 300 ms compared to windows of 0 or 600 ms leads us to speculate that the former is a more physiologically relevant period for neuronal integration.

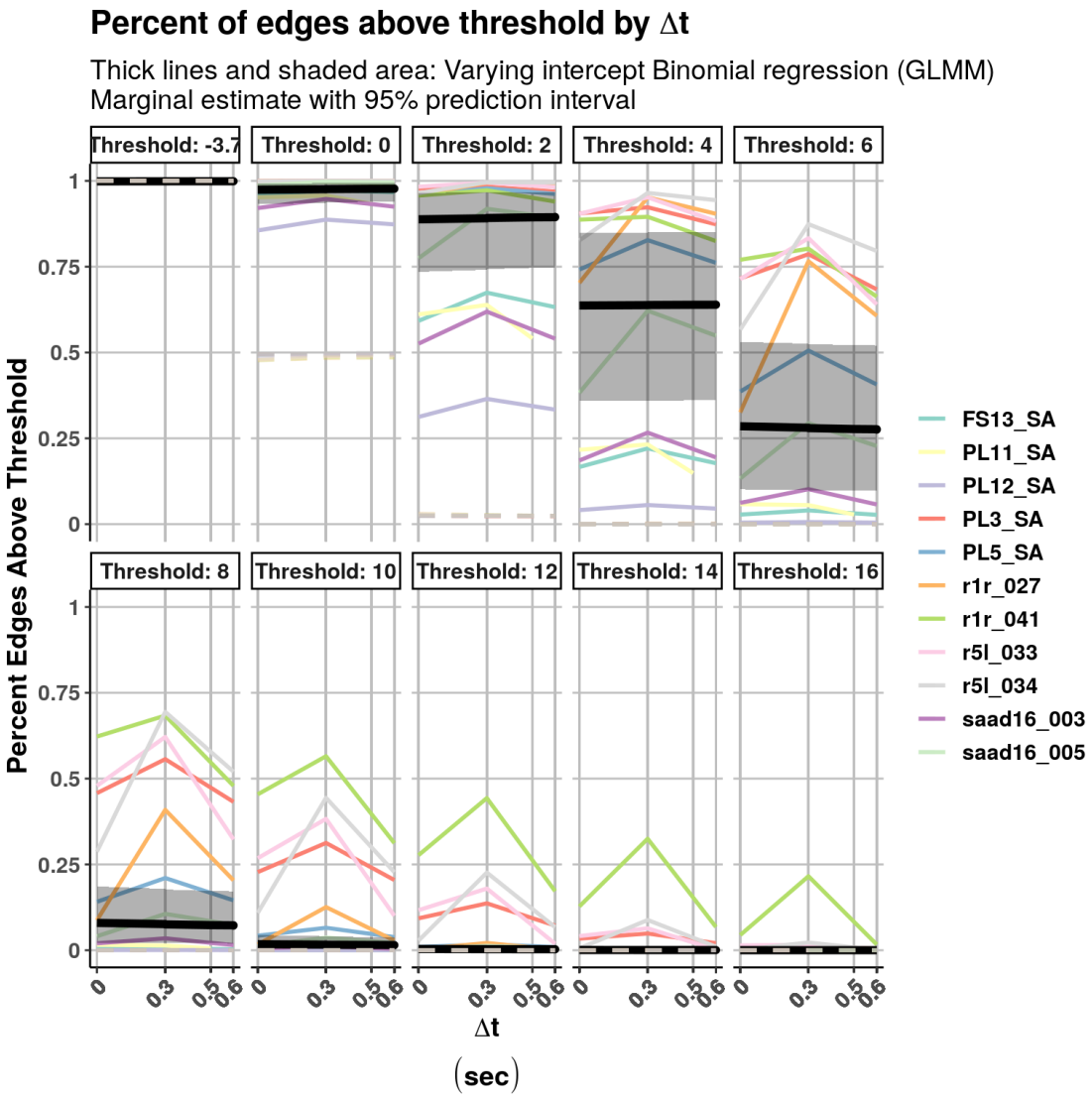

Figure 5: ***Percent of edges above different thresholds by*** *Δt: The dashed lines represent the median percentage of edges above different thresholds for the synthetic values, which are equal for all FOVs up to the third decimal point and close to the percentiles of the Normal distribution. The model is specified in equation (4).*

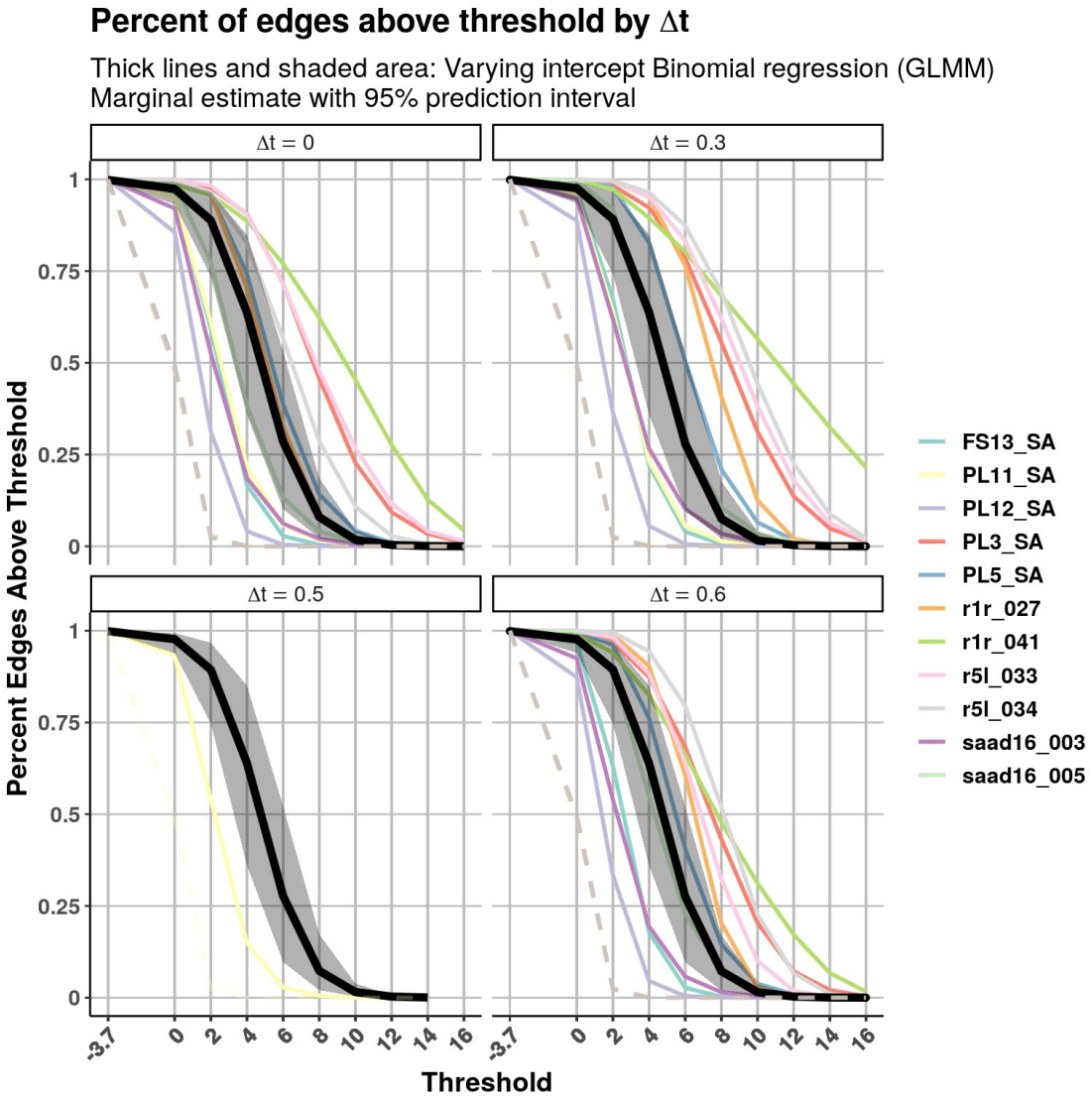

Figure 6: ***Percent of edges above threshold by*** *Δt: The dashed lines represent the median percentage of edges above different thresholds for the synthetic values, which are equal for all FOVs up to the third decimal point and close to the percentiles of the Normal distribution. The model is specified in equation (4).*

4. No apparent hubs based on the degree distribution; Networks do not resemble Erdös-Rényi networks based on the average path length and the average clustering coefficient

A basic characteristic of a network is its degree of connectivity distribution, which provides a description of how many edges each node has within the network. Typically, a hub is a node with a degree of connectivity significantly larger than the mean degree of connectivity. The observed degree distributions in the neuronal networks we recorded have no overlap for positive Z-thresholds with those

produced based on the shifted firing events, which only reach to degrees up to 4 (data not shown). Hence, the number of edges is at least an order of magnitude more that those we would expect due to correlations between neurons with the same number of firing events we observed but without the observed temporal structure. The degree distribution of the observed network is heavily shaped by the choice of Z-threshold, ranging from a distribution with most nodes having a large degree for low thresholds to most nodes having a small degree for high thresholds (Figure 7). For thresholds for which the network was not fully connected, as exhibited by degree distributions that are not concentrated around the largest possible number of edges, the degree distribution did not resemble an equivalent Erdös-Rényi (ER) network (Figure 8). This indicates that there were proportionally more neurons with fewer as well as with more connections than expected in an equivalent ER network.

However, there is an apparent lack of “hub”-neurons, i.e. those that would exhibit a distinctly larger degree compared to the rest of the population.

Given the unstructured connectivity the ER network is built on, it is possible in such a network to reach any node starting from any other node with relatively few edge crossings. We can quantify this network property as the average shortest path length, i.e. the average number of edges between each node and all other nodes of the network. Since we constructed the equivalent ER networks based on the number of nodes and edges of the observed networks but without any information regarding the inter-node correlation, we should expect that the average shortest path will monotonically increase as we increase the threshold. Both the observed and their equivalent ER networks are characterized by relatively short average shortest path lengths for low Z-thresholds (Figure 9). However, as the threshold increases, the average shortest path length of the equivalent ER networks increases with a higher rate compared to the observed network (Median average shortest path length for observed: 1.90, simulated: 2.77) and this was true for all fields of view (FOV)/mice, as can be observed by inspecting the median average shortest path length for the observed and the equivalent ER networks across thresholds for all FOVs (Figure 10). This indicates that the observed networks contain enough nodes that are highly correlated with many other neurons to act as “bridges” between neurons that are themselves not connected with each other. Both the observed and the equivalent networks show a sharp drop of their median average shortest path after they reach their peak, as the number of nodes is reduced so much that most nodes can be connected with each other simply due to the small number of nodes.

Another important parameter of a network is its average node clustering coefficient, which quantifies the percentage of a node’s neighbours that are connected. Equivalent ER networks should have a relatively small average clustering coefficient that should drop monotonically as the Z-threshold, and hence the number of nodes and edges, is decreased. We observe that for all FOVs/mice we examined the average clustering coefficient of the observed networks falls at a relatively slow rate compared to their equivalent ER networks, and in some cases even stabilizes or increases (Figure 11). This evidence suggests that the observed networks are more

tightly connected compared to their equivalent ER networks. In FOVs/mice where the average clustering coefficient stabilizes or increases, it signifies that the network possesses a core of highly correlated neurons, which are not encountered in equivalent ER networks.

(ref:degreeCDFUndirectedByFOVAndThresholdPlot) **Undirected degree CDF per FOV by Z-threshold for all animals**: The data presented were processed with $\Delta t = 0.3$.

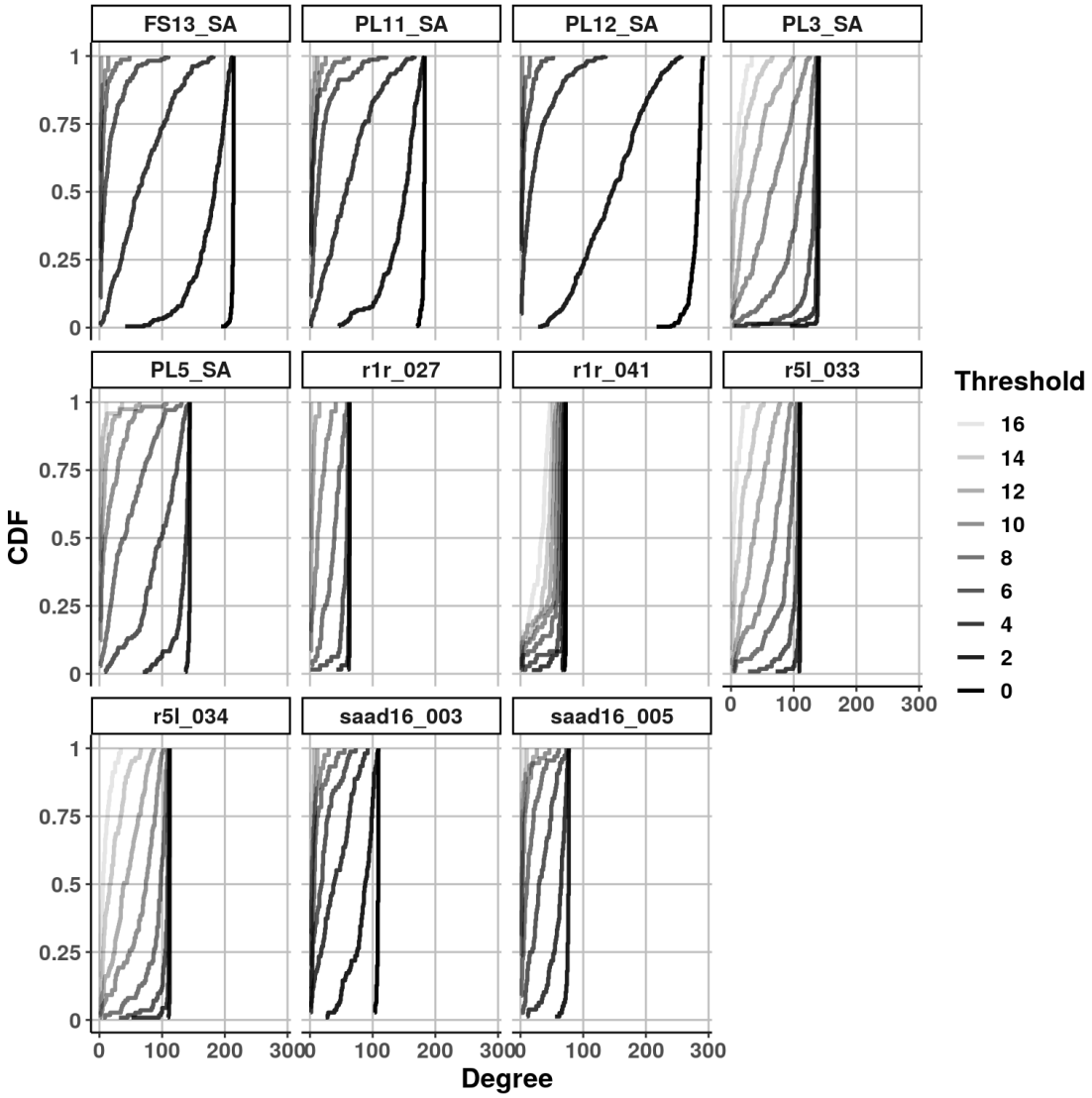

Figure 7: (ref:degreeCDFUndirectedByFOVAndThresholdPlot)

(ref:exampleMouseUndirectedDegreeWithShuffled) **Undirected degree CDF per FOV by Z-threshold for an example animal**: The data presented were processed with $\Delta t = 0.3$.

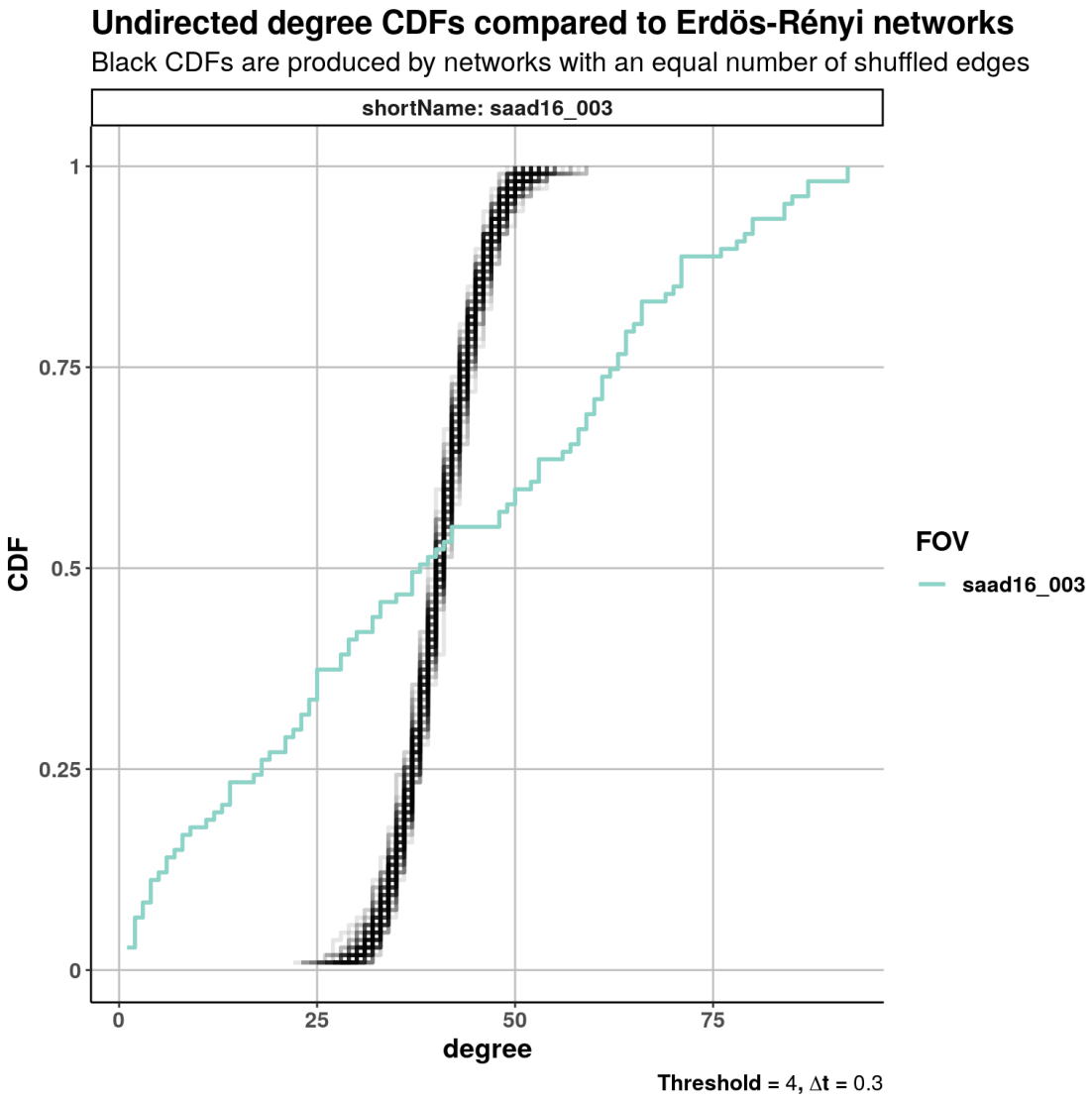

Figure 8: (ref:exampleMouseUndirectedDegreeWithShuffled)

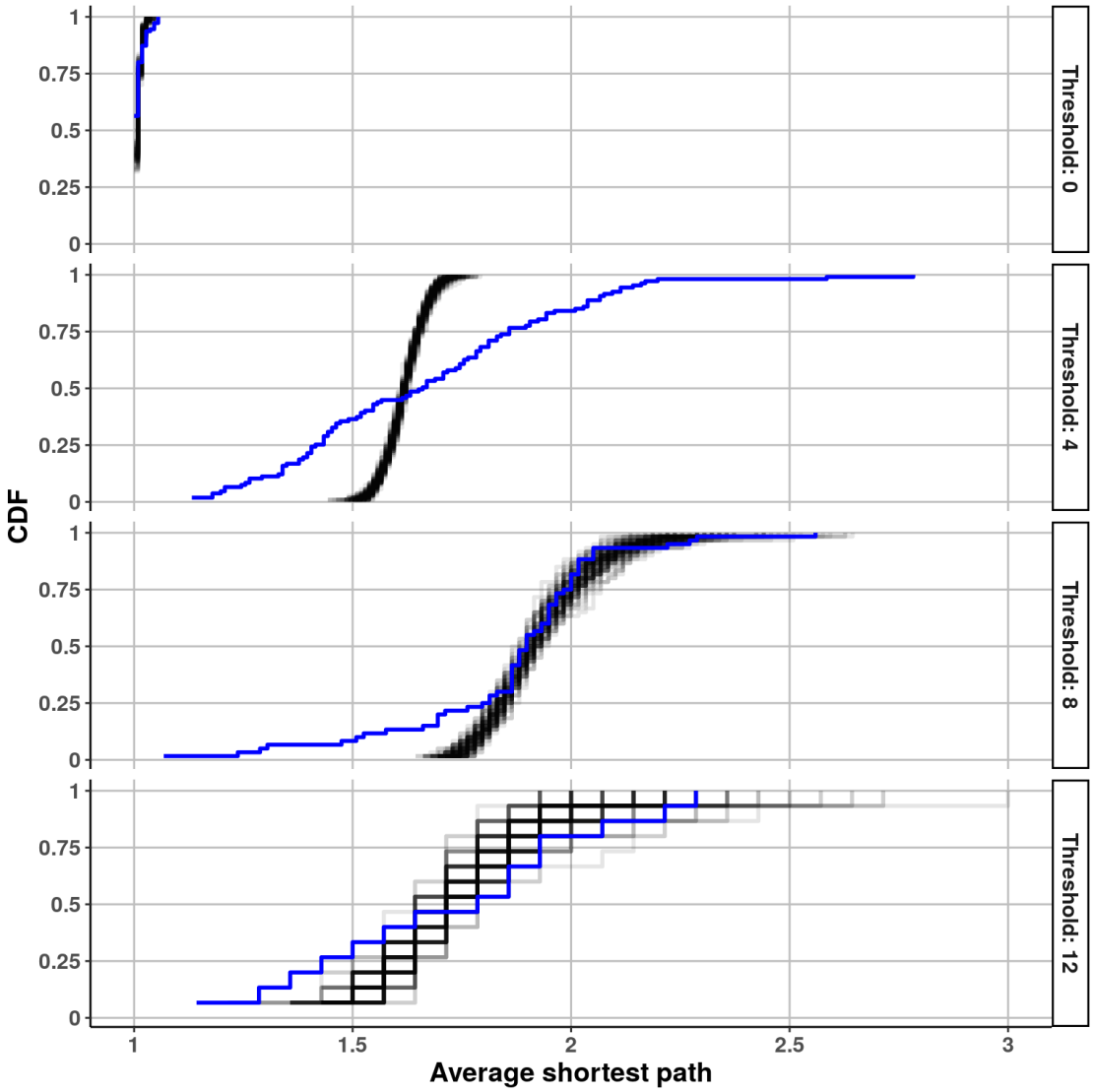

Figure 9: ***Average shortest path length for an example mouse compared with shuffled edges networks****: The STTC has been calculated with* $\Delta t \approx 0.3$.

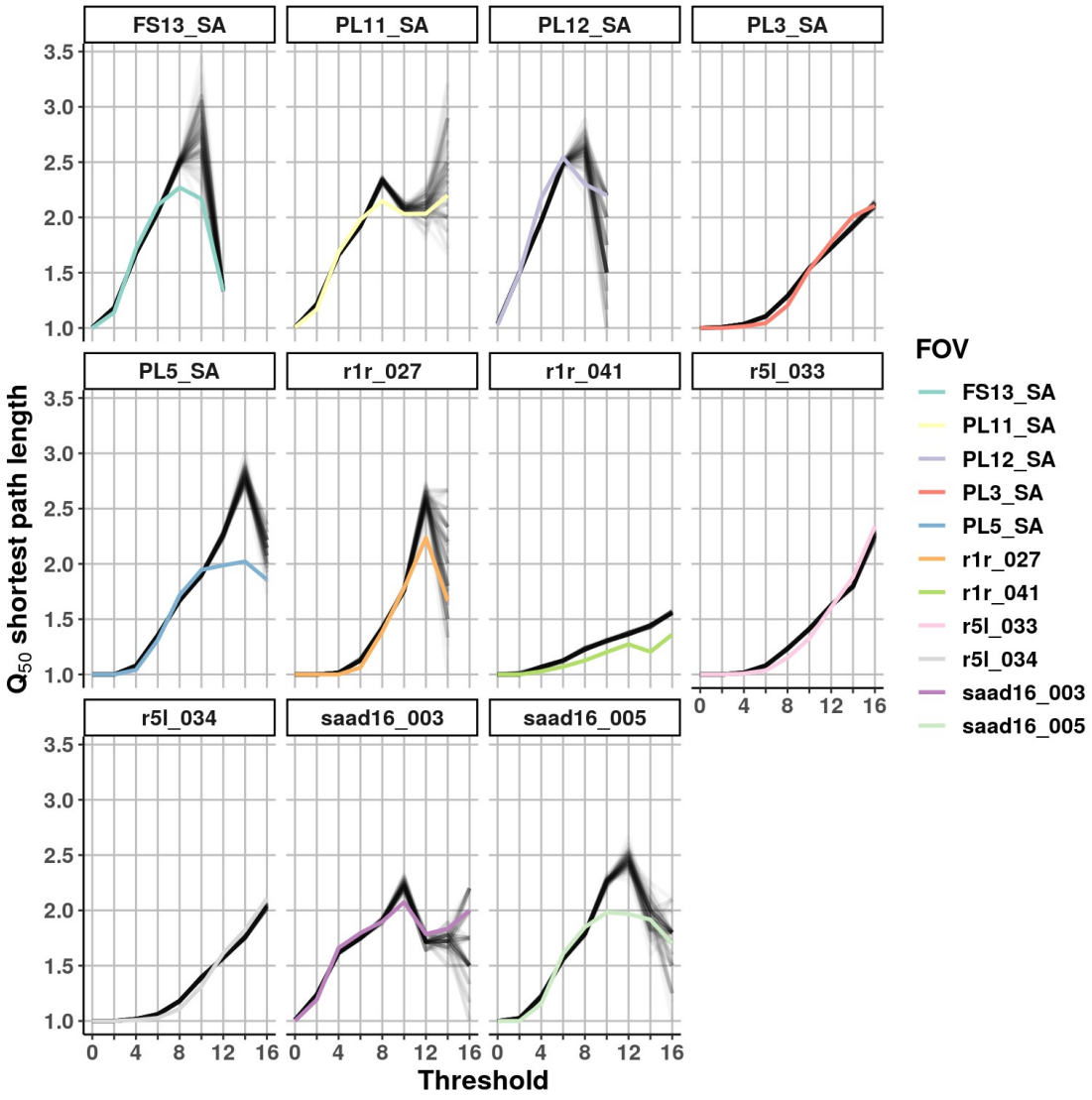

Figure 10: ***Median undirected shortest path length per FOV by*** *Z-threshold: The coloured CDFs represent the observed data and the corresponding CDFs (N = 100) generated by an equivalent Erdös-Rényi network (equal number of nodes and shuffled edges) are shown in black. The data presented, for both observed and shuffled data, were processed with* $\Delta t \approx 0.3$.

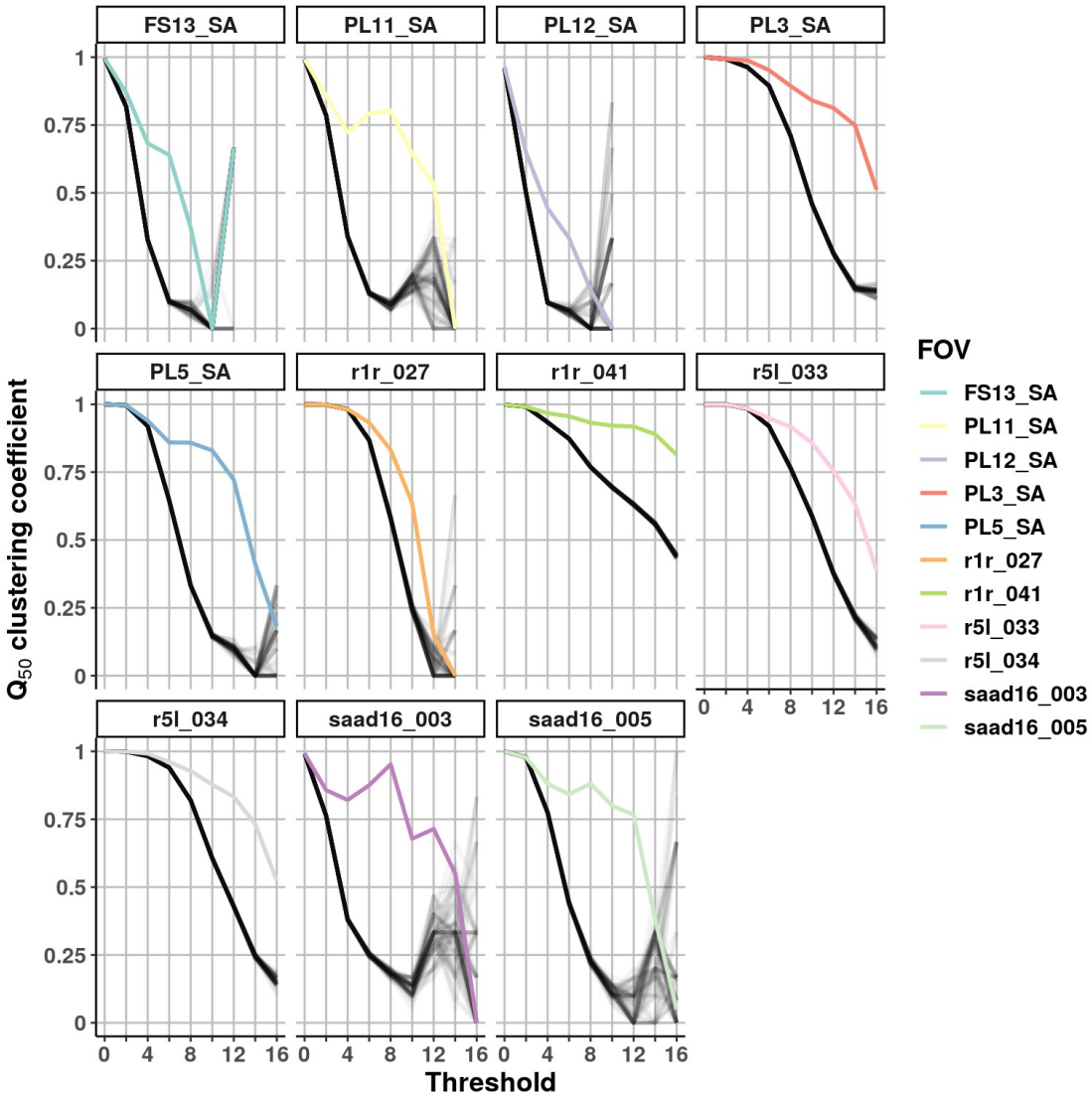

Figure 11: ***Median undirected node clustering coefficient with shuffled****: The coloured lines represent the observed data and the corresponding lines (N = 100) generated by an equivalent Erdös-Rényi network (equal number of nodes and shuffled edges) are shown in black. The data presented, for both observed and shuffled data, were processed with* $\Delta t = 0.3$.

Small-worldness in the observed networks.

The observed networks display properties that cannot be found in equivalent ER networks: degree distributions with more variance, shorter average shortest path lengths, and larger clustering coefficients. These properties can be found in so-called "small-world" networks (Watts and Strogatz 1998) that can be created by rewiring a proportion of edges of a network based on a fixed probability of rewiring, p. At the one extreme, when the Watts-Strogatz algorithm starts with a highly regular

network such as a ring lattice network where each node is connected with an equal number of its closest neighbours, each node has high clustering coefficient and large shortest path lengths. If $p=1$, all edges will be rewired to connect uniformly selected nodes, resulting in "random" ER networks, where each node has small clustering coefficient and small average shortest path lengths, provided that there are enough nodes in the network. For a range of intermediate values for p, an interesting phenomenon occurs, where the network is able to retain the lattice's high clustering coefficient to a large extend while it also reaches a small average shortest path length similarly to the ER network. Networks in this regime are called small-world networks, and are thought to arise spontaneously under certain conditions leading to robust self-organization.

To quantify the small-worldness of the observed networks, we employed the ω small-world inxex (Telesford et al. 2011). The basic idea behind this index is to compare the observed clustering coefficient and shortest paths with those of reference lattice and "random" networks, against which to assess the network's regularity and lack of structure, respectively. When ω is close to 0, the network is considered small-world. When it is negative, it approaches closer to the lattice network used and when it is positive, it approaches closer to the "random" network used. In our case, all FOVs display ω values that are typically positive but always smaller than those obtained by the equivalent ER graphs for all thresholds tested for which they diverge, indicating that the observed graphs display more structured connectivity patterns than expected for equivalent ER networks, a result that was confirmed with two other small-world indices [LINK TO APPENDIX].

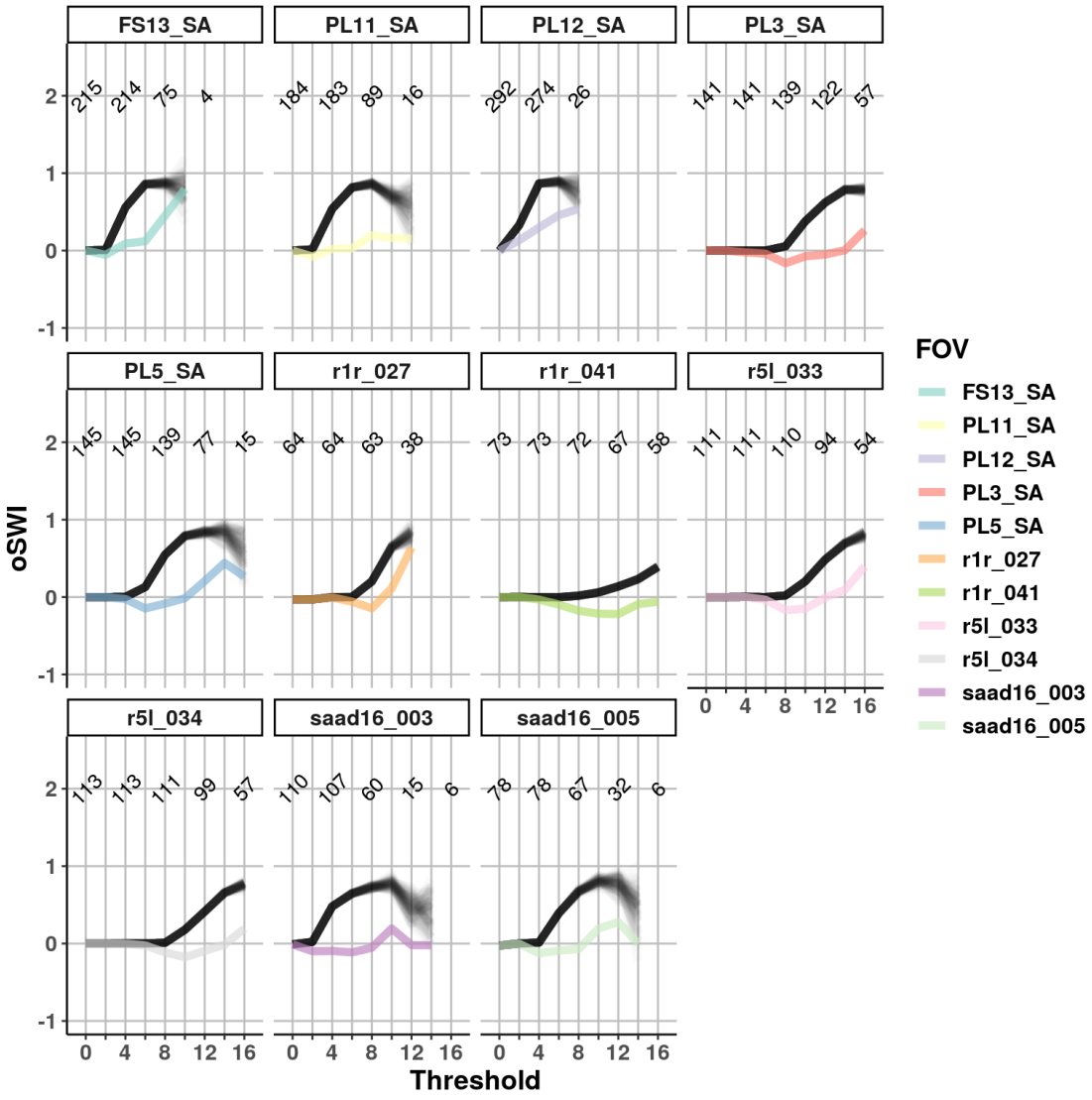

Figure 12: ***Small world index*** ω ***over thresholds****: The simulated shuffled graphs were generated based on the original data processed with* $\Delta t \approx 0.3$*. The random graph used is constructed using the Erdös-Rényi algorithm and the lattice is a ring lattice. Each colour line is calculated using the observed data and the mean clustering coefficient of all shuffled graphs. Each black line uses each of the shuffled graphs instead of the observed data. The text within each panel plot area indicates the number of connected nodes per threshold. For visual clarity, every other number has been skipped where they would overlap.*

Differences between mice/ mesoscope

Equivalent results can be confirmed from recordings of a large L2/3 neuronal population in an awake mouse

The number of neurons we recorded from some mice of those we presented so far appeared to be limited, as shown by the fact that many neurons exhibited the maximum possible degree, even when setting high Z-thresholds (Figure 7). A further limitation may have been that all the animals were anaesthetized during the recordings. We thus confirmed our previous findings with mesoscopic data, from awake mice where we recorded thousands of neurons, thus expecting that the influence of both limitations will be alleviated. The mesoscopic data include recordings of 5205 neurons from layer $(L)2/3$ from mouse $V\,1$. The median $STTC_{\Delta t \approx 0.3}$ value for this animal was ≈ 0.01 with $\approx 8\,\%$ of values ¿ 0.1. In this mouse as well, we see that the degree distribution displays differing proportions of low- and high-degree nodes, based on the applied Z-threshold (Figure 13). Predictably, the clustering coefficient distribution is shifted to lower values and the average shortest path distribution is shifted to higher values as we increase the Z-threshold. For this mouse as well, we wondered how much different the observed network is compared to an equivalent ER network. As with all other mice, the observed average clustering coefficient was larger than that of the ER network for all thresholds tested (Figure 14). Similarly, the median shortest path length of the ER network increased at a higher rate compared to the observed network (Figure 15). Following this evidence, we found that the ω small-world index for this network as well was kept below that of the ER network (Figure 16), indicating that the observed network follows closer the small-world topology compared to the ER network.

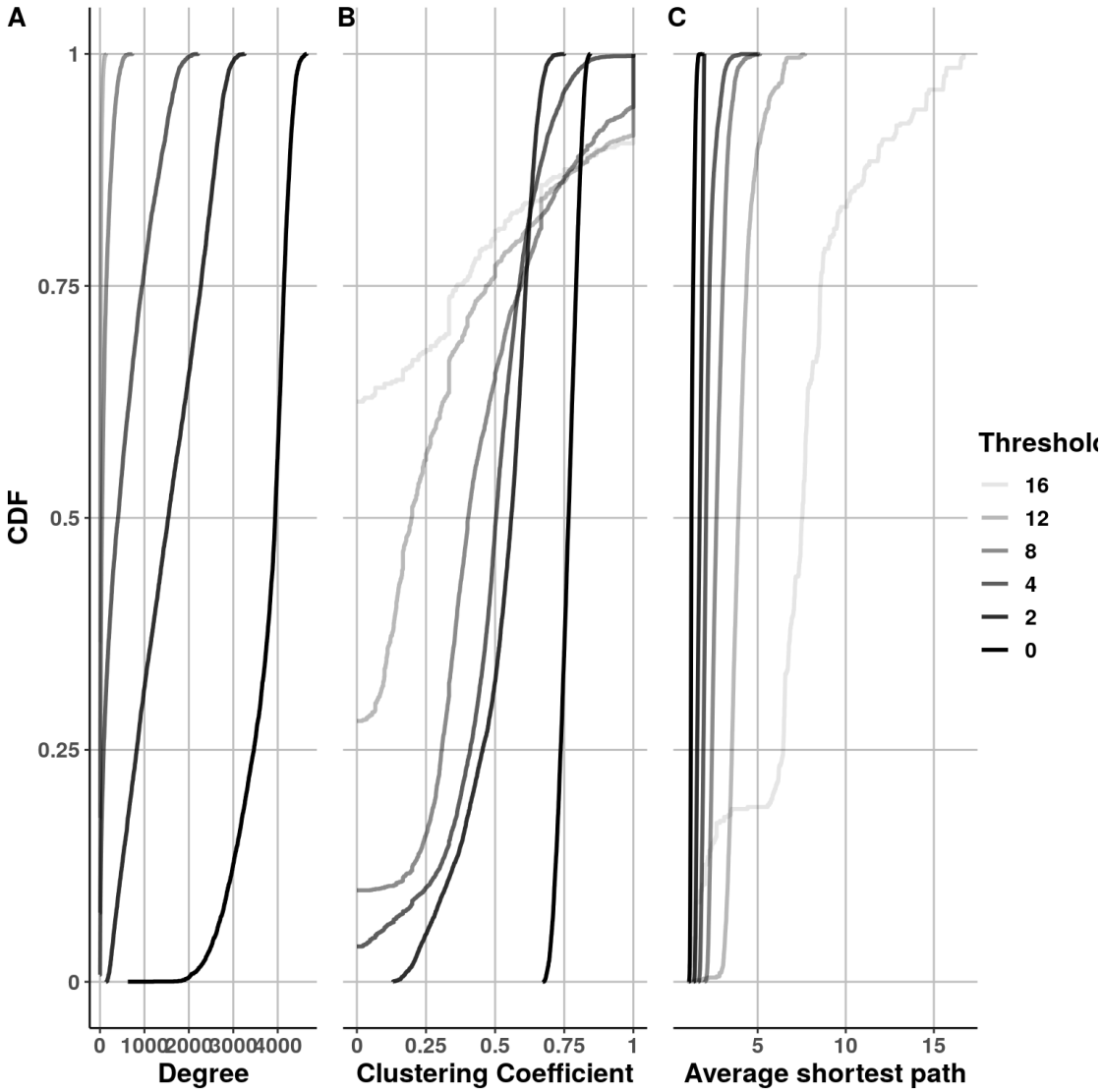

Figure 13: ***Graph metrics for mesoscope L2/3 network****: A) Undirected degree CDF, B) Undirected clustering coefficient CDF, C) Undirected average shortest path CDF. For these calculations, paths greater than 100 edges were set to infinite distances to reduce computation time and hence were excluded from this distribution plots. However, all neurons for which the average shortest path is not defined have a degree of* 0 *so this cut-off should not affect the results.*

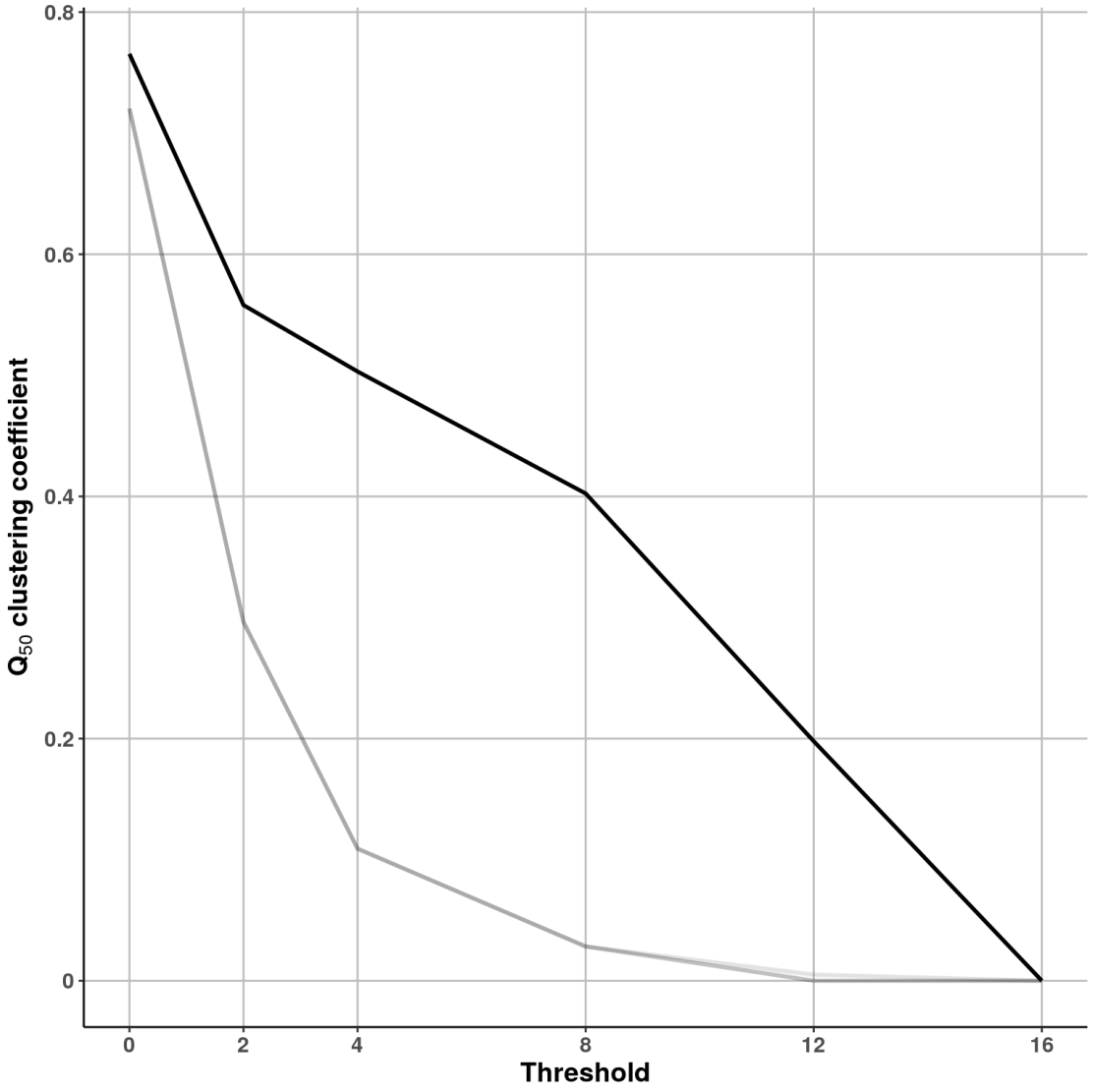

Figure 14: ***Median clustering coefficient from mesoscope L2/3 data with shuffled graph****: The black line represents the results of the observed graph and the grey lines those from* 10 *equivalent shuffled graphs.*

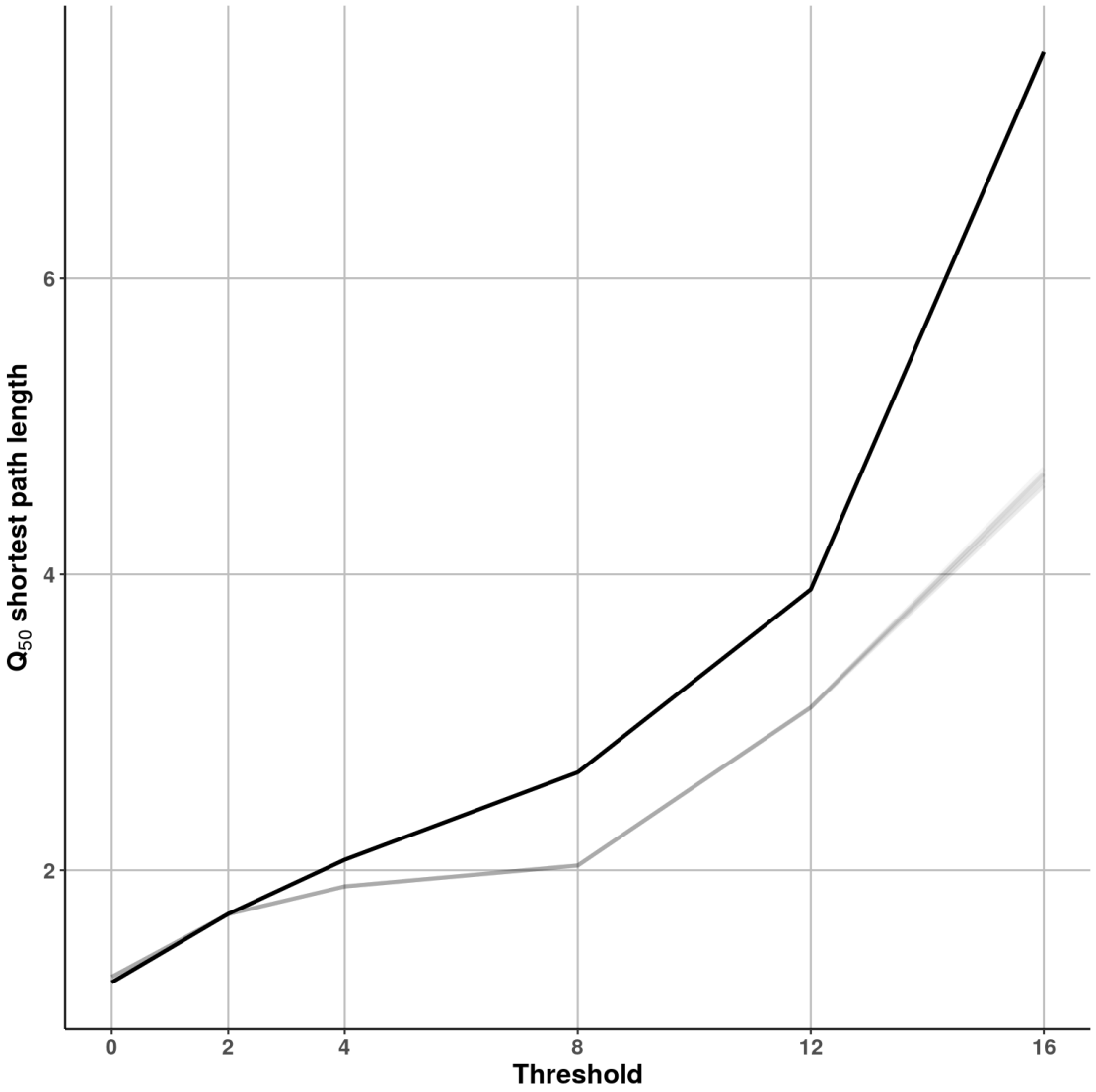

Figure 15: ***Median average shortest path from mesoscope L2/3 data with shuffled graph****: The black line represents the results of the observed graph and the grey lines those from* 10 *equivalent shuffled graphs.*

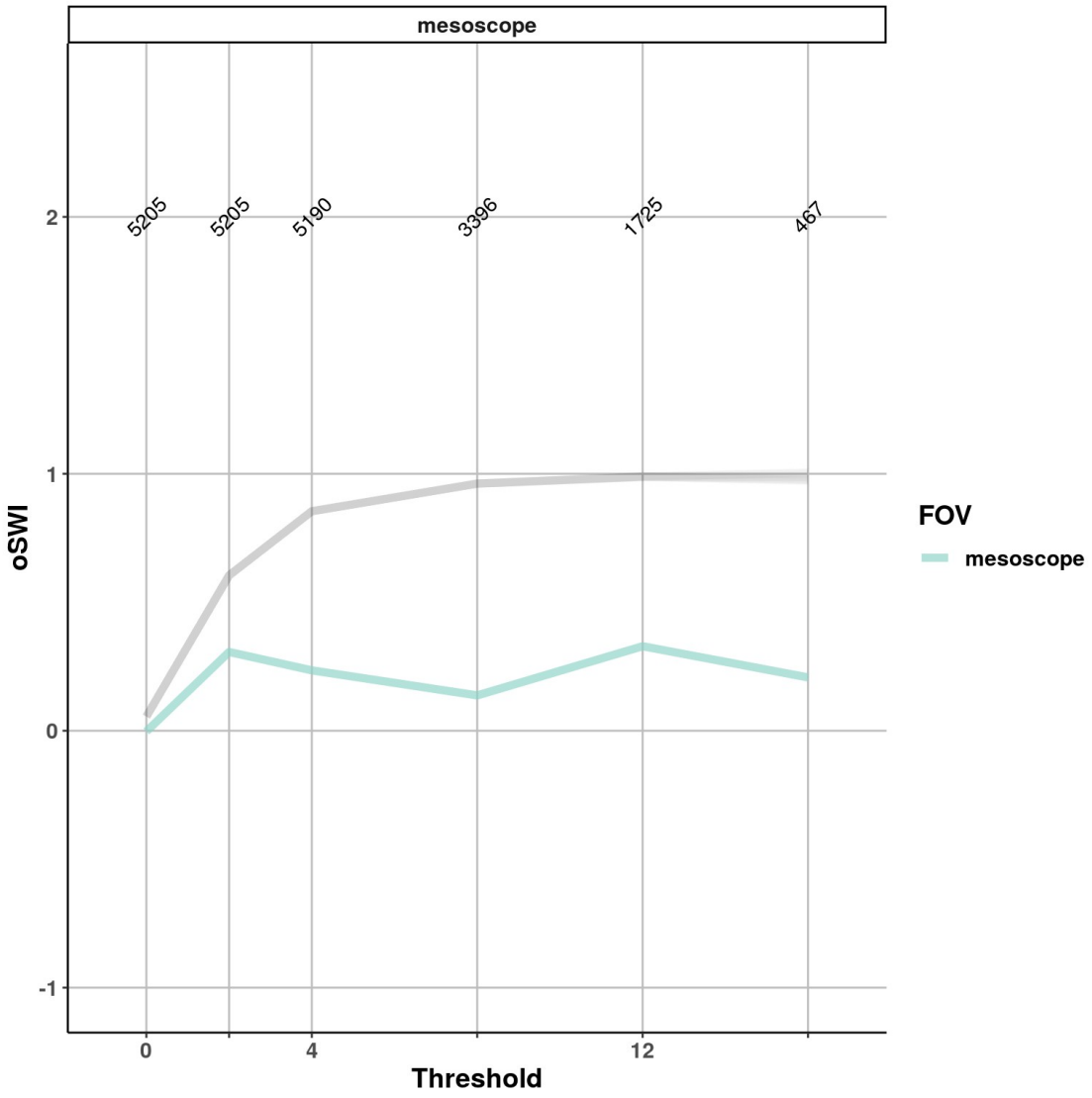

Figure 16: ***Small world index*** ω ***over thresholds for mesoscope data****: The coloured line represents the observed data and the grey lines the* 10 *shuffled graphs.*

Survival by degree

The lack of clear hub neurons raises the question of which neurons sustain the small-world network. To investigate this, we plotted the survival of individual nodes that were sorted according to their degree as we increase the Z-threshold (Figure 17). As expected, we can first observe that high-degree neurons tend to be those that survive up to the highest threshold. Additionally, we observe that node clustering coefficient correlates with node degree, with high-degree neurons tending to have high clustering coefficient as well. It is interesting, however, that as the threshold increases the neurons with the highest clustering coefficient are not those with the highest degree but those that are rather close to the median degree. High-degree neurons also tend to have the smallest average shortest paths. Those

neurons with intermediate degrees and high clustering coefficients display increasingly large average shortest paths, until they run out of strongly correlated connections as we increase the threshold.

It appears, then, that neurons with intermediate clustering coefficients are well-connected in small neighbourhoods but less so with the rest of the network, as indicated by their increasing average shortest path as the Z-threshold increases. In contrast, the nodes of highest degree, may not participate in the most tightly connected networks, perhaps also as a consequence of their high degree, but at least some of their connections are formed by edges of high correlations. However, the network as a whole was, in this example case, contained within one connected component for all Z-thresholds. The above results are also observed with data from other mice and are largerly confirmed with the mesoscope data as well (Figure 18).

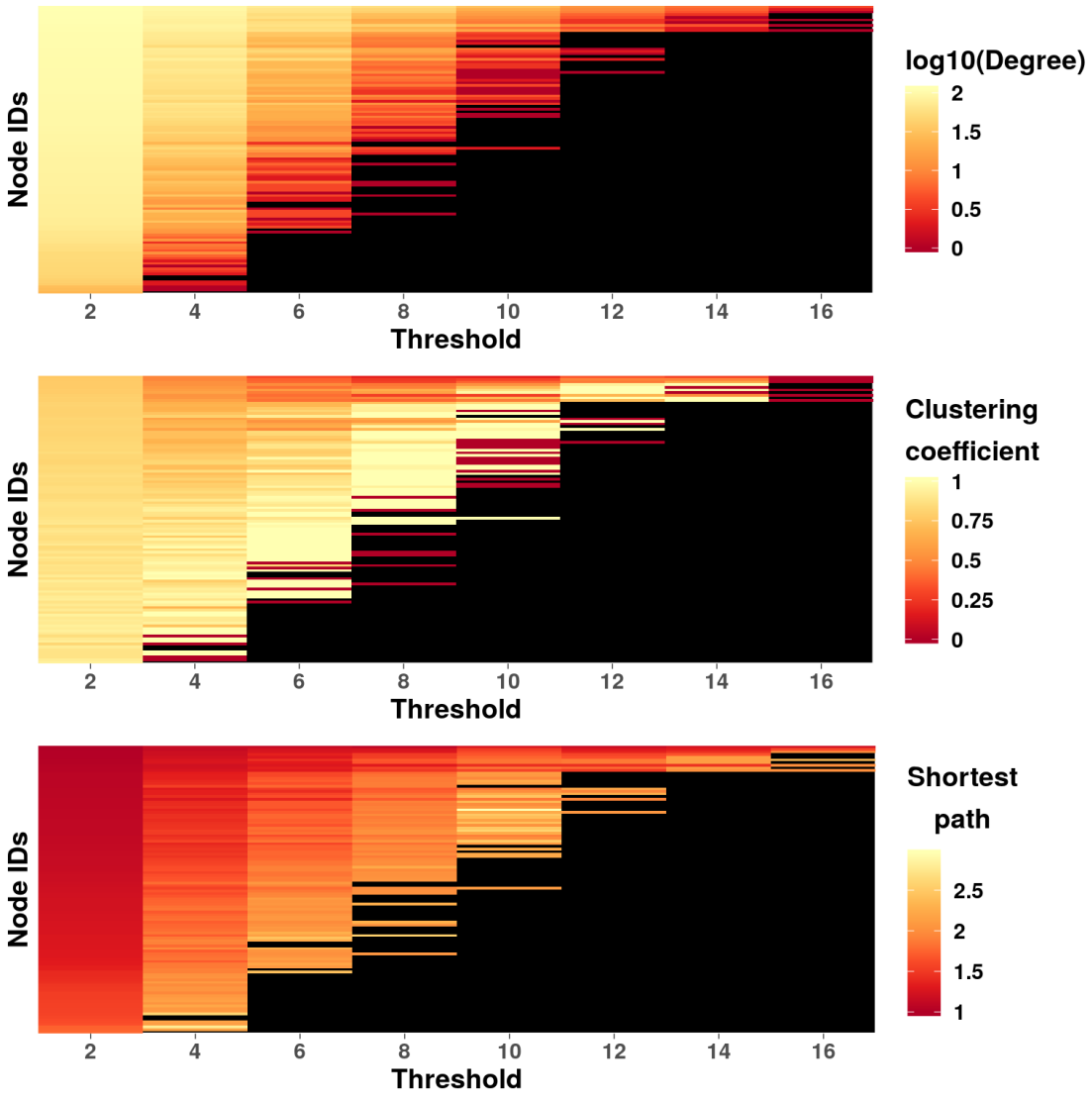

Figure 17: ***Node survival at increasing thresholds for mouse saad16_003****: The nodes in all panels are sorted according to their degree for each successive threshold and each row represents one node. A black line denotes absence.*

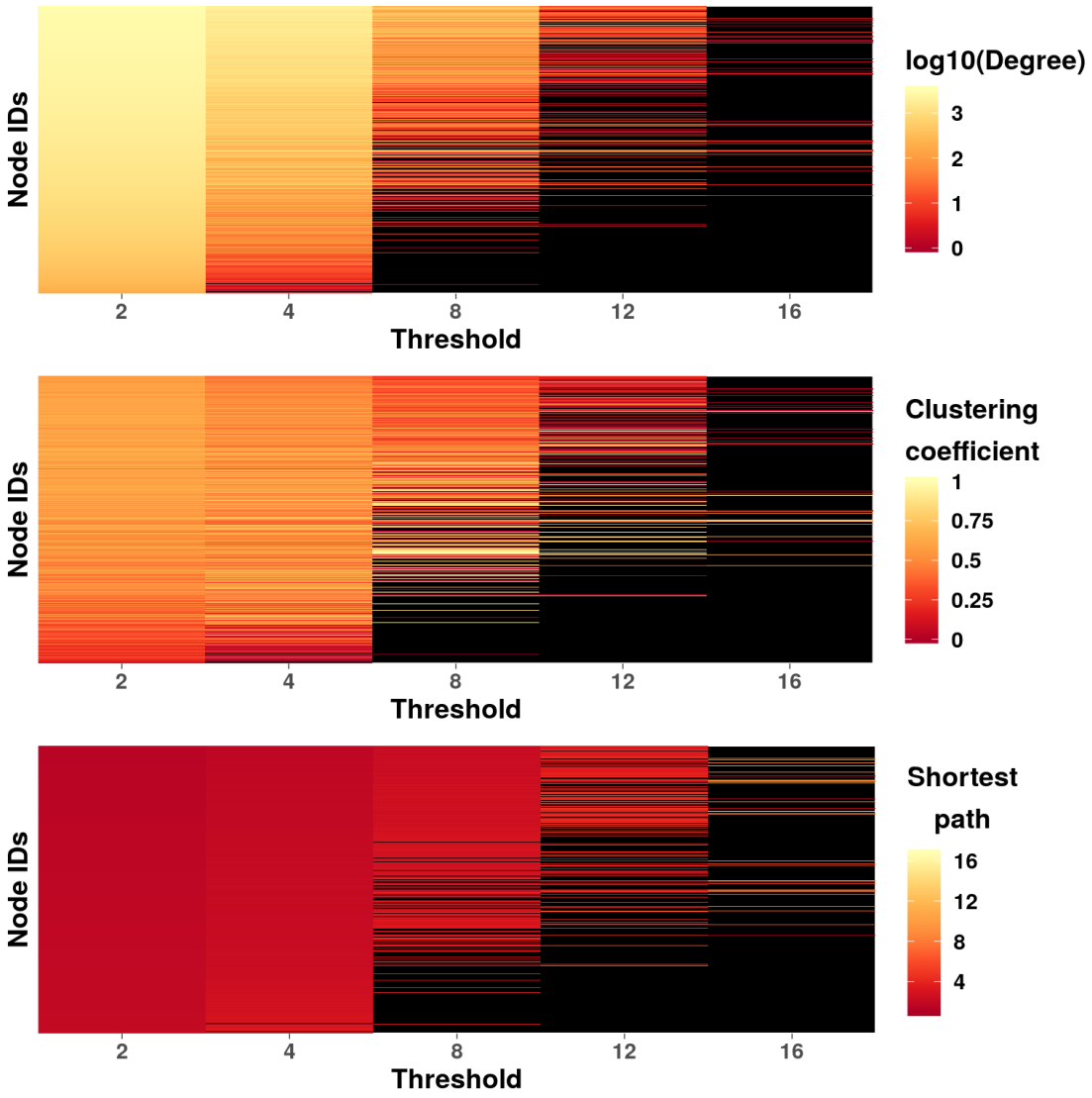

Figure 18: ***Node survival at increasing thresholds for the mesoscope mouse****: The nodes in all panels are sorted according to their degree for each successive threshold and each row represents one node. A black line denotes absence.*

Discussion

Summary

- There is temporal structure in the data
- The temporal structure is more obviously manifested with shorter time-scales (Δt)

- The temporal structure manifests irrespective of the correlation scale at which we choose to look at the network

- At high-correlation scales the networks are not well-described by the ER topology but rather resemble a small-world topology with no apparent hubs

- The observed small-world topology is subsisted by a sub-group of neurons which are tightly connected in almost all-to-all neighbourhoods

Conclusions

We analyzed spontaneous L2/3 cortical activity through calcium imaging of large neuronal populations. The STTC-based method of correlation estimation robustly identifies correlated pairs of neurons. Although, on average, there is little correlation between neurons, cortical networks display considerable temporal structure at all correlation thresholds. Within a range of temporal integration windows, correlation saturates for windows ~300ms, in agreement with the literature (Smith and Kohn 2008). The observed networks tend to have smaller average shortest path lengths and larger average clustering coefficients compared to equivalent reference networks with shuffled edges, manifesting small-world architecture. These trends persist at various correlation thresholds. Furthermore, the presence of sub-groups of tightly-connected neurons indicating that cortical networks are built based on a modular structure.

References

Braitenberg, Valentino, and Almut Schüz. 1998. *Cortex: Statistics and Geometry of Neuronal Connectivity*. Berlin, Heidelberg: Springer Berlin Heidelberg. https://doi.org/10.1007/978-3-662-03733-1.

Chen, Tsai-Wen, Trevor J. Wardill, Yi Sun, Stefan R. Pulver, Sabine L. Renninger, Amy Baohan, Eric R. Schreiter, et al. 2013. "Ultrasensitive Fluorescent Proteins for Imaging Neuronal Activity." *Nature* 499 (7458): 295–300. https://doi.org/10.1038/nature12354.

Cohen, Marlene R, and Adam Kohn. 2011. "Measuring and Interpreting Neuronal Correlations." *Nature Neuroscience* 14 (7): 811–19. https://doi.org/10.1038/nn.2842.

Cossell, Lee, Maria Florencia Iacaruso, Dylan R. Muir, Rachael Houlton, Elie N. Sader, Ho Ko, Sonja B. Hofer, and Thomas D. Mrsic-Flogel. 2015. "Functional Organization

of Excitatory Synaptic Strength in Primary Visual Cortex." *Nature* 518 (7539): 399–403. https://doi.org/10.1038/nature14182.

Cutts, Catherine S., and Stephen J. Eglen. 2014. "Detecting Pairwise Correlations in Spike Trains: An Objective Comparison of Methods and Application to the Study of Retinal Waves." *The Journal of Neuroscience* 34 (43): 14288–14303. https://doi.org/10.1523/JNEUROSCI.2767-14.2014.

Ecker, A.S., P. Berens, G.A. Keliris, M. Bethge, N.K. Logothetis, and A.S. Tolias. 2010. "Decorrelated Neuronal Firing in Cortical Microcircuits." *Science* 327 (5965): 584–87. https://doi.org/10.1126/science.1179867.

Humphries, Mark D., and Kevin Gurney. 2008. "Network 'Small-World-Ness': A Quantitative Method for Determining Canonical Network Equivalence." Edited by Olaf Sporns. *PLoS ONE* 3 (4): e0002051. https://doi.org/10.1371/journal.pone.0002051.

Ko, Ho, Sonja B. Hofer, Bruno Pichler, Katherine A. Buchanan, P. Jesper Sjöström, and Thomas D. Mrsic-Flogel. 2011. "Functional Specificity of Local Synaptic Connections in Neocortical Networks." *Nature* 473 (7345): 87–91. https://doi.org/10.1038/nature09880.

Madisen, Linda, Theresa A. Zwingman, Susan M. Sunkin, Seung Wook Oh, Hatim A. Zariwala, Hong Gu, Lydia L. Ng, et al. 2010. "A Robust and High-Throughput Cre Reporting and Characterization System for the Whole Mouse Brain." *Nature Neuroscience* 13 (1): 133–40. https://doi.org/10.1038/nn.2467.

Miyoshi, Goichi, Jens Hjerling-Leffler, Theofanis Karayannis, Vitor H. Sousa, Simon J. B. Butt, James Battiste, Jane E. Johnson, Robert P. Machold, and Gord Fishell. 2010. "Genetic Fate Mapping Reveals That the Caudal Ganglionic Eminence Produces a Large and Diverse Population of Superficial Cortical Interneurons." *Journal of Neuroscience* 30 (5): 1582–94. https://doi.org/10.1523/JNEUROSCI.4515-09.2010.

Neal, Zachary P. 2017. "How Small Is It? Comparing Indices of Small Worldliness." *Network Science* 5 (1): 30–44. https://doi.org/10.1017/nws.2017.5.

Palagina, Ganna, Jochen F. Meyer, and Stelios M. Smirnakis. 2019. "Inhibitory Units: An Organizing Nidus for Feature-Selective SubNetworks in Area V1." *Journal of Neuroscience* 39 (25): 4931–44. https://doi.org/10.1523/JNEUROSCI.2275-18.2019.

Perin, R., T. K. Berger, and H. Markram. 2011. "A Synaptic Organizing Principle for Cortical Neuronal Groups." *Proceedings of the National Academy of Sciences* 108 (13): 5419–24. https://doi.org/10.1073/pnas.1016051108.

Renart, A., J. de la Rocha, P. Bartho, L. Hollender, N. Parga, A. Reyes, and K. D. Harris. 2010. "The Asynchronous State in Cortical Circuits." *Science* 327 (5965): 587–90. https://doi.org/10.1126/science.1179850.

Ringach, Dario L. 2009. “Spontaneous and Driven Cortical Activity: Implications for Computation.” *Current Opinion in Neurobiology*, Sensory systems, 19 (4): 439–44. https://doi.org/10.1016/j.conb.2009.07.005.

Schneider, Caroline A., Wayne S. Rasband, and Kevin W. Eliceiri. 2012. “NIH Image to ImageJ: 25 Years of Image Analysis.” *Nature Methods* 9 (June): 671–75. https://doi.org/10.1038/nmeth.2089.

Smith, M. A., and A. Kohn. 2008. “Spatial and Temporal Scales of Neuronal Correlation in Primary Visual Cortex.” *Journal of Neuroscience* 28 (48): 12591–12603. https://doi.org/10.1523/JNEUROSCI.2929-08.2008.

Song, Sen, Per Jesper Sjöström, Markus Reigl, Sacha Nelson, and Dmitri B. Chklovskii. 2005. “Highly Nonrandom Features of Synaptic Connectivity in Local Cortical Circuits.” *PLOS Biology* 3 (3): e68. https://doi.org/10.1371/journal.pbio.0030068.

Stosiek, Christoph, Olga Garaschuk, Knut Holthoff, and Arthur Konnerth. 2003. “In Vivo Two-Photon Calcium Imaging of Neuronal Networks.” *Proceedings of the National Academy of Sciences* 100 (12): 7319–24. https://doi.org/10.1073/pnas.1232232100.

Stringer, Carsen, Marius Pachitariu, Nicholas Steinmetz, Charu Bai Reddy, Matteo Carandini, and Kenneth D. Harris. 2019. “Spontaneous Behaviors Drive Multidimensional, Brainwide Activity.” *Science* 364 (6437): eaav7893. https://doi.org/10.1126/science.aav7893.

Telesford, Qawi K., Karen E. Joyce, Satoru Hayasaka, Jonathan H. Burdette, and Paul J. Laurienti. 2011. “The Ubiquity of Small-World Networks.” *Brain Connectivity* 1 (5): 367–75. https://doi.org/10.1089/brain.2011.0038.

Truccolo, Wilson, Leigh R. Hochberg, and John P. Donoghue. 2010. “Collective Dynamics in Human and Monkey Sensorimotor Cortex: Predicting Single Neuron Spikes.” *Nature Neuroscience* 13 (1): 105–11. https://doi.org/10.1038/nn.2455.

Vogelstein, Joshua T., Adam M. Packer, Timothy A. Machado, Tanya Sippy, Baktash Babadi, Rafael Yuste, and Liam Paninski. 2010. “Fast Nonnegative Deconvolution for Spike Train Inference from Population Calcium Imaging.” *Journal of Neurophysiology* 104 (6): 3691–3704. https://doi.org/10.1152/jn.01073.2009.

Wang, Quanxin, and Andreas Burkhalter. 2007. “Area Map of Mouse Visual Cortex.” *Journal of Comparative Neurology* 502 (3): 339–57. https://doi.org/10.1002/cne.21286.

Watts, Duncan J., and Steven H. Strogatz. 1998. “Collective Dynamics of ‘Small-World’ Networks.” *Nature* 393 (6684): 440–42. https://doi.org/10.1038/30918.

Yoshimura, Yumiko, Jami L. M. Dantzker, and Edward M. Callaway. 2005. “Excitatory Cortical Neurons Form Fine-Scale Functional Networks.” *Nature* 433 (7028): 868–73. https://doi.org/10.1038/nature03252.

Yu, Shan, Debin Huang, Wolf Singer, and Danko Nikolić. 2008. “A Small World of Neuronal Synchrony.” *Cerebral Cortex* 18 (12): 2891–2901. https://doi.org/10.1093/cercor/bhn047.

Yu, Yong-Chun, Ronald S. Bultje, Xiaoqun Wang, and Song-Hai Shi. 2009. “Specific Synapses Develop Preferentially Among Sister Excitatory Neurons in the Neocortex.” *Nature* 458 (7237): 501–4. https://doi.org/10.1038/nature07722.

Zador, Anthony M. 2019. “A Critique of Pure Learning and What Artificial Neural Networks Can Learn from Animal Brains.” *Nature Communications* 10 (1): 1–7. https://doi.org/10.1038/s41467-019-11786-6.